Clathrin-Mediated Endocytosis of Quantum Dot–Peptide Conjugates in Living Cells

Abdulaziz Anas,[§] Tetsuya Okuda, Nagako Kawashima, Kenichi Nakayama, Tamitake Itoh, Mitsuru Ishikawa,[†,‡] and Vasudevanpillai Biju[§,†,*]

Nanobioanalysis Team and Glycolipid Function Analysis Team, Health Technology Research Center, National Institute of Advanced Industrial Science and Technology (AIST), 2217-14 Hayashi-Cho, Takamatsu, Kagawa 761-0395, Japan. [†]Also at Center for Arthropod Bioresources and Biotechnology, Kerala University, Kariavattom, India. [‡]Also at Kwansei Gakuin University, Sanda, Japan (ishikawa-mitsuru@aist.go.jp). [§]These authors contributed equally to this work.

ABSTRACT Efficient intracellular delivery of quantum dots (QDs) and unravelling the mechanism underlying the intracellular delivery are essential for advancing the applications of QDs toward *in vivo* imaging and therapeutic interventions. Here, we show that clathrin-mediated endocytosis is the most important pathway for the intracellular delivery of peptide-conjugated QDs. We selected an insect neuropeptide, namely, allatostatin (AST1, APSGAQRLYG FGL-NH_2), conjugated it with CdSe–ZnS QDs, and investigated the intracellular delivery of the conjugate in living cells such as human epidermoid ovarian carcinoma cells (A431) and mouse embryonic fibroblast cells (3T3). We selected AST1 to investigate the intracellular delivery of QDs because we recently found it to be efficient for delivering QDs in living mammalian cells. Also, the receptors of AST1 in insects show functional and sequence similarity to G-protein-coupled galanin receptors in mammals. We employed flow cytometry and fluorescence microscopy and investigated the contributions of clathrin-mediated endocytosis, receptor-mediated endocytosis, and charge-based cell penetration or transduction to the intracellular delivery of QD–AST1 conjugates. Interestingly, the intracellular delivery was suppressed by ~57% when we inhibited the regulatory enzyme phosphoinositide 3-kinase (PI3K) with wortmannin and blocked the formation of clathrin-coated vesicles. In parallel, we investigated clathrin-mediated endocytosis by colocalizing QD560-labeled clathrin heavy-chain antibody and QD605–AST1. We also estimated galanin receptor-mediated endocytosis of QD–AST1 at <10% by blocking the cells with a galanin antagonist and transduction at <30% by both removing the charge of the peptide due to arginine and suppressing the cell-surface charge due to glycosaminoglycan. In short, the current work shows that multiple pathways are involved in the intracellular delivery of peptide-conjugated QDs, among which clathrin-mediated endocytosis is the most important.

KEYWORDS: quantum dots · peptide · endocytosis · transduction · clathrin · living cells · phosphoinositide 3-kinase

Biological applications of semiconductor quantum dots (QDs) are translating from bioanalysis to *in vivo* imaging[1−15] and photodynamic therapy[16−18] since Bruchez *et al.*[19] and Chan and Nie[20] demonstrated cell imaging using bioconjugated QDs. Bright and stable emission and broad absorption and narrow emission bands of QDs are attractive properties for multiplexed detection of biomolecules[19−26] and multicolor imaging cells,[1,10,27−36] tissues, and whole animals[1−8,37] for extended periods of time. Also, noninvasive imaging of tumor vasculature[1,3,14,15,38] and lymph nodes[1,3,6−8] are two recent achievements owing to the large two-photon absorption cross section of QDs and the introduction of NIR QDs.[3,8,37,39,40] Recently, the potential of QDs for photodynamic therapy of cancer was recognized when photosensitized energy transfer from QD was realized.[16−18] However, the *in vitro* and *in vivo* imaging and therapeutic applications of QDs are limited by their poor intracellular delivery and aggregation.[1,10,21,23,30,32,41−45] The intracellular delivery of QDs depends on many factors such as size, surface charge, and surface functionality.[46] Different techniques investigated for the intracellular delivery of QDs were electroporation,[47] microinjection,[13] and biochemical techniques.[1,30,38,44,47,48] Generally, QDs delivered in cells by physical methods aggregate in the cytosol due to endosomal arrest, which was considerably resolved by Nie and co-workers by encapsulating QDs in a polyethylene glycol grafted polyethyleneimine.[32,42] More recently, Weng *et al.* successfully targeted QDs in tumor cells using multifunctional immunoliposomes.[49] Similarly, Yong *et al.* demonstrated that InP QDs conjugated with anticlaudin 4 and antiprostate stem cell antigen were efficiently delivered in pancreatic cancer cells.[50] Yet another promising approach for the intracellular delivery of QDs is coating/conjugating QDs with phospholipids.[1,10,11,13,51] Despite all these advancements, due to bioavailability and cost effectiveness, peptides are promising candidates for the intracellular delivery of QDs.[10,12,26,38,41−45,48,52−55] Nevertheless, the intracellular trafficking of many peptide-conjugated QDs are limited due to aggregation.

*Address correspondence to v.biju@aist.go.jp.

Received for review June 24, 2009 and accepted July 27, 2009.

Published online August 4, 2009. 10.1021/nn900663r CCC: $40.75

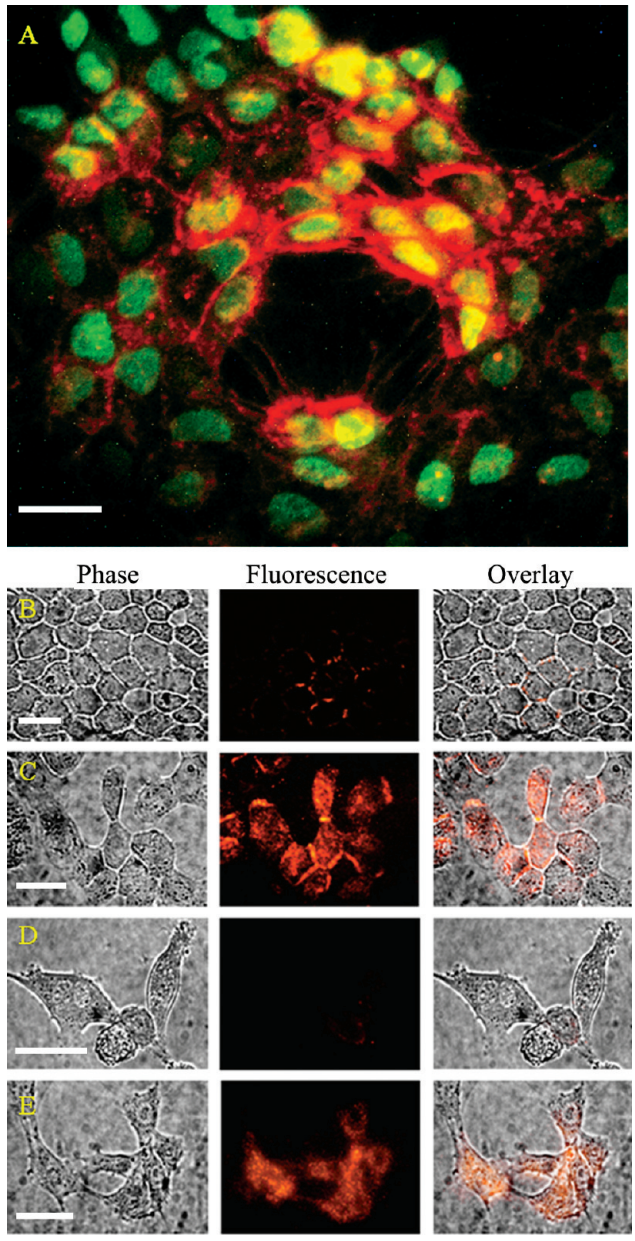

Figure 1. (A) Fluorescence image of A431 cells incubated with a 5 μM Syto16 dye solution for 10 min followed by a 1 nM QD605−AST1 solution for 30 min. Cell nucleus is preferentially stained green by Syto16 due to its cell permeability and DNA intercalation. The yellow-orange color indicates colocalized QD−AST1 and Syto16. (B−E) Phase, fluorescence, and overlay images of (B,C) A431 and (D,E) 3T3 cells labeled using solutions of (B,D) 0.5 nM QD−streptavidin and (C,E) 0.5 nM QD−AST1. The scale bars are 25 μm. Note that all of the images were equally corrected for brightness and contrast.

One of the main challenges in the cell biological and *in vivo* applications of peptide-conjugated QDs is that the mechanism underlying the intracellular delivery of QD−peptide conjugates remains largely unknown. Cell-penetrating cationic peptides such as polyarginines,[44,48] polylysines,[56] tryptophan-rich peptides,[57] and Tat peptides[12,38,43] were widely investigated for the intracellular delivery of QDs. Two mechanisms, endocytosis and transduction, were proposed to account for the intracellular delivery of cell-penetrating peptides.[41,42,44,51,58,59] Recently, Chen *et al.* found that the intracellular delivery of a QD−Tat conjugate took place through lipid-raft-dependent macropinocytosis.[61] Endocytosis is mediated by cell-surface receptors and clathrin protein.[57,59,62] The general mechanism underlying clathrin-mediated endocytosis is that the extracellular molecules such as peptides, proteins, ligands, and localized receptors are encapsulated into clathrin-coated pits and subsequently taken up in the form of clathrin-coated vesicles. The heterodimeric regulatory enzyme phosphoinositide 3-kinase (PI3K) is essential for assembling clathrin protein into clathrin-coated vesicles;[63] PI3K is activated during the translocation of autophosphorylated growth factor receptors. On the other hand, transduction takes place through either a direct cell penetration or an inverted micelle formation due to the charge, hydrophobicity, and hydrogen bonding ability of a peptide.[58,59] For example, the intracellular delivery of arginine-rich peptides is initiated by a charge-based interaction with the plasma membrane followed by the formation of a bidentate hydrogen bond between the guanidine group in the peptide and the phospholipid head groups in the plasma membrane,[64] but tryptophan-rich peptides attach to the plasma membrane through hydrophobic interactions.[65] Thus, the intracellular delivery of a peptide or a peptide-conjugated QD varies with the structure and the physicochemical properties of the peptide.

To account for what mechanism is important in the intracellular delivery of QDs by peptides, we selected an insect neuropeptide, namely, allatostatin (AST1, APSGAQRLYG FGL-NH_2),[66,67] conjugated it with CdSe−ZnS QDs, and investigated the intracellular delivery of the conjugate in living A431 and 3T3 cells. AST1 belongs to the allatostatin family of 13 neuropeptides, bearing 8−13 amino acids and conserved C termini (YXFGL-NH_2), which are widely distributed in insects and crustaceans.[66,67] We selected AST1 because we recently found that it efficiently delivered QDs in living mammalian cells.[55] Also, DAR1 and DAR2 receptors of AST1 in insects and crustaceans show functional and sequence similarity to G-protein-coupled galanin receptors in mammals.[66,68] Here, we investigated clathrin-mediated endocytosis, galanin receptor-mediated endocytosis, and charge-based cell penetration or transduction to account for the intracellular delivery of QD−AST1. We investigated clathrin-mediated endocytosis by inhibiting PI3K with wortmannin, a cell-permeable steroidal furanoid that irreversibly inhibits PI3K,[63] and by colocalizing clathrin heavy-chain antibody and QD−AST1. We also investigated the contributions of galanin receptor-mediated endocytosis by blocking the cells with a galanin antagonist and transduction by both incubating the cells with QDs conjugated with an AST1 mutant in which the positive charge of AST1 was removed by replacing the arginine unit with an alanine unit (MAST1, APSGAQALYG FGL-NH_2) and suppressing the cell-

surface charge due to glycosaminoglycan by preincubating the cells with heparinase enzyme.[69] On the basis of these investigations, we arrived at the conclusion that multiple pathways are involved in the intracellular delivery of QD−AST1, among which clathrin-mediated endocytosis is the most important.

RESULTS AND DISCUSSION

We prepared two QD−peptide conjugates, QD−AST1 and QD−MAST1, by simple biotin−streptavidin linkage. The peptides were biotinylated using biotin *N*-hydroxysuccinimide (NHS) ester and subsequently conjugated to streptavidin-functionalized QDs (QD605) at a 1:5 molar ratio (QD/peptide). We selected this ratio to improve the intracellular delivery of QDs. Nanoparticles conjugated with multiple peptides were efficiently delivered in living cells.[39] We cultured human epidermoid ovarian carcinoma cells (A431) and mouse embryonic fibroblast cells (3T3) up to 50% confluencies and incubated with 1 nM solutions of QD−peptide conjugates. Intracellular delivery of the conjugates was investigated using fluorescence microscopy. Here, we selected two different cell lines to test the general nature of the intracellular delivery of QD−AST1. Figure 1A shows the fluorescence image of A431 cells incubated with a 5 μM Syto16 dye solution for 10 min followed by a 1 nM QD−AST1 solution for 30 min. Nuclei of the cells were stained green by cell-permeable Syto16. The yellow-orange color in Figure 1A is due to QDs and Syto16 colocalized in the nucleus. Initially, we detected the QD−AST1 conjugates on the cell membrane, and with time under incubation, the conjugates were transported into the cytoplasm and nucleus. Figure 1B−E shows phase, fluorescence, and overlay images of A431 and 3T3 cells incubated with QD−AST1 and QD−streptavidin conjugates (control). Figure 1B,D shows that the control QDs sparsely labeled the cell membrane. On the other hand, Figure 1C,E shows that QD−AST1 conjugates were efficiently delivered inside the cells. Note that any significant difference in the intracellular delivery and distribution of QD−AST1 between A431 and 3T3 cells are probably due to different cell structure and physiology.[62] The efficient intracellular delivery of QD−AST1 in A431 and 3T3 cells, which is consistent with our previous work,[55] indicates that AST1 is a potential carrier of nanoparticles and therapeutic macromolecules. Thus, a detailed investigation of how QD−AST1 conjugates were delivered in living cells is relevant not only to understand the mechanism underlying the intracellular delivery of bioconjugated nanoparticles but also to advance the cell biological applications of nanoparticles, as well.

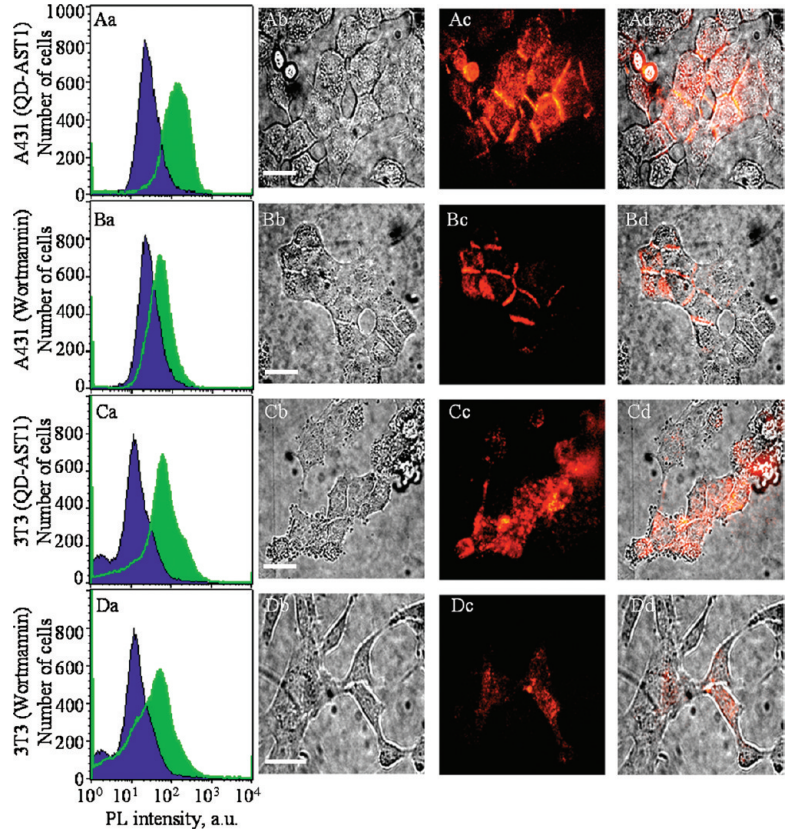

Figure 2. (Column a) Flow cytometry histograms, (column b) optical transmission images, (column c) fluorescence images, and (column d) overlaid images of A431 and 3T3 cells: (panel A) A431 cells incubated with a 1 nM QD−AST1 solution, (panel B) A431 cells incubated with a 50 nM wortmannin solution followed by a 1 nM QD−AST1 solution, (panel C) 3T3 cells incubated with a 1 nM QD−AST1 solution, (panel D) 3T3 cells incubated with a 50 nM wortmannin solution followed by a 1 nM QD−AST1 solution. The scale bars are 25 μm. Note that all of the images were equally corrected for brightness and contrast.

To investigate the mechanism underlying the intracellular delivery of QD−AST1, we recorded and analyzed the flow cytometry histograms and fluorescence images of A431 and 3T3 cells under various conditions for blocking the endocytosis and transduction. We investigated the contribution of clathrin-mediated endocytosis to the intracellular delivery of QD−AST1 by inhibiting the regulatory kinase PI3K with wortmannin. Figure 2 shows the flow cytometry histograms and the fluorescence images of cells incubated with QD−AST1 before (panels A and C) and after (panels B and D) inhibiting PI3K with a 50 nM wortmannin solution. Also, bars "a" and "b" in Figure 3 show the efficiency for the intracellular delivery of QD−AST1 before and after incubating the cells with wortmannin. Interestingly, the efficiency of the intracellular delivery was decreased for the cells preincubated with wortmannin; the number of cells with fluorescence was decreased by 57 ± 5% (bar b in Figure 3). On the basis of the flow cytometry values and the average fluorescence intensity of cells, it is apparent that blocking the formation of clathrin-coated vesicles by inhibiting PI3K resulted in a consid-

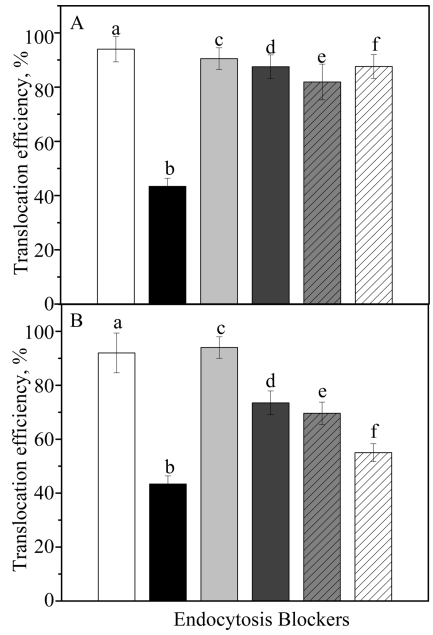

Figure 3. Fluorescence intensity distributions for (A) A431 and (B) 3T3 cells incubated with solutions of (a) 1 nM QD−AST1, (b) 50 nM wortmannin followed by 1 nM QD−AST1, (c) 100 nM galanin receptor antagonist followed by 1 nM QD−AST1, (d) 1 nM QD−MAST1, (e) 0.5 U heparinase enzyme followed by 1 nM QD−AST1, and (f) 1 nM QD−AST1 at 4 °C. The fluorescence intensity values were measured for 5 × 10^4 to 1 × 10^5 cells in each flow cytometry experiment. The difference in the fluorescence intensity values in A and B was probably due to the structural and physiological differences between A431 and 3T3 cells.

erable decrease in the intracellular delivery of QD−AST1. Wortmannin is a cell-permeable steroidal furanoid, which irreversibly inhibits PI3K by blocking its ATP binding pocket and modifying the lysine side chain at the P110 catalytic subunit into a vinylogous carbamate.[63] Although wortmannin has many other inhibitory functions *in vivo* at elevated concentrations (μM), such as the inhibition of various kinases, NADPH oxidase, interleukin-8, platelet-derived growth factor receptor, histamine release, insulin-stimulated glucose uptake, nerve growth factor-dependent survival, differentiation, and platelet aggregation,[63] at concentrations as low as 50 nM, wortmannin is unlikely to interfere much with the cell physiology, but PI3K, which is essential for assembling clathrin protein into clathrin-coated vesicles. Therefore, the decrease in the fluorescence of cells preincubated with wortmannin suggested that clathrin-mediated endocytosis contributed 57 ± 5% to the intracellular delivery of QD−AST1.

To further investigate clathrin-mediated endocytosis of QD−AST1, we examined the colocalization of clathrin heavy-chain antibody and QD−AST1 using flow cytometry and fluorescence microscopy. The antibody was biotinylated using biotin sulfo-NHS ester and subsequently conjugated with green fluorescent QDs (QD560, $\lambda_{max} \sim 560$ nm) through biotin−streptavidin linkage. A431 and 3T3 cells were incubated with solutions (equivalent to 1 nM QD560) of the labeled antibody for 30 min, copiously washed with PBS, and incubated with 1 nM QD−AST1 (QD605) solution for 30 min. Figure 4 shows the flow cytometry histograms and fluorescence images of A431 cells incubated with the QD560−antibody (green) and QD605−AST1 (red) conjugates. Compared with the fluorescence intensity of cells incubated with QD560−antibody (trace b in Figure 4A), a considerable (>200%) increase in the fluorescence intensity was observed for the cells incubated with QD560−antibody + QD605−AST1 (trace c in Figure 4A), indicating that the cells were efficiently labeled with both QD560−antibody and QD605−AST1 conjugates. Also, Figure 4B−E shows optical transmission image and fluorescence images of A431 cells treated with the QD−antibody and QD−AST1 conjugates. The overlaid image (Figure 4E) shows that the QD−antibody and QD−AST1 conjugates were efficiently colocalized. In other words, QD−AST1 was colocalized with clathrin-coated vesicles, suggesting that clathrin-mediated endocytosis considerably contributed to the intracellular delivery of QD−AST1. Although clathrin heavy-chain antibody specifically binds with the intracellular clathrin protein, how the QD−antibody conjugate penetrated the plasma membrane of living cells and labeled the intracellular clathrin protein was unknown. Thus, we further investigated the colocalization of QD560−antibody and QD605−AST1 conjugates after permeabilizing the cell membrane. For this, living A431 cells were incubated with QD605−AST1 (1 nM) for 30 min at room temperature, copiously washed with PBS, and the medium was exchanged with 99.5% ice-cold methanol. The cells were incubated in methanol for 10 min at −20 °C, rinsed with PBS, and blocked in a blocking buffer. The blocking solution was aspirated, and the cells were incubated in a QD−antibody solution (1 nM) and copiously washed with PBS. Figure 4F−H shows the fluorescence images of membrane permeabilized cells. We found that essentially all of the QD605−AST1 conjugates (red fluorescence) were colocalized with the QD560−antibody conjugates (green fluorescence), suggesting that clathrin-mediated endocytosis considerably contributed to the intracellular delivery of QD−AST1. In general, clathrin-mediated endocytosis takes place by encapsulating the extracellular molecules such as peptides, proteins, ligands, and oligomerized receptors into clathrin-coated pits followed by internalization in the form of clathrin-coated vesicles.[60,62] Therefore, on the basis of the PI3K inhibition assay and the colocalization of QD−AST1 and clathrin antibody, we attribute that clathrin-mediated endocytosis played an important role in the intracellular delivery of QD−AST1. Figure 5 shows schematic presentation of clathrin-mediated endocytosis of QD−AST1.

To investigate the contribution of galanin receptor-mediated endocytosis to the intracellular delivery of QD−AST1, we blocked the galanin receptors in A431

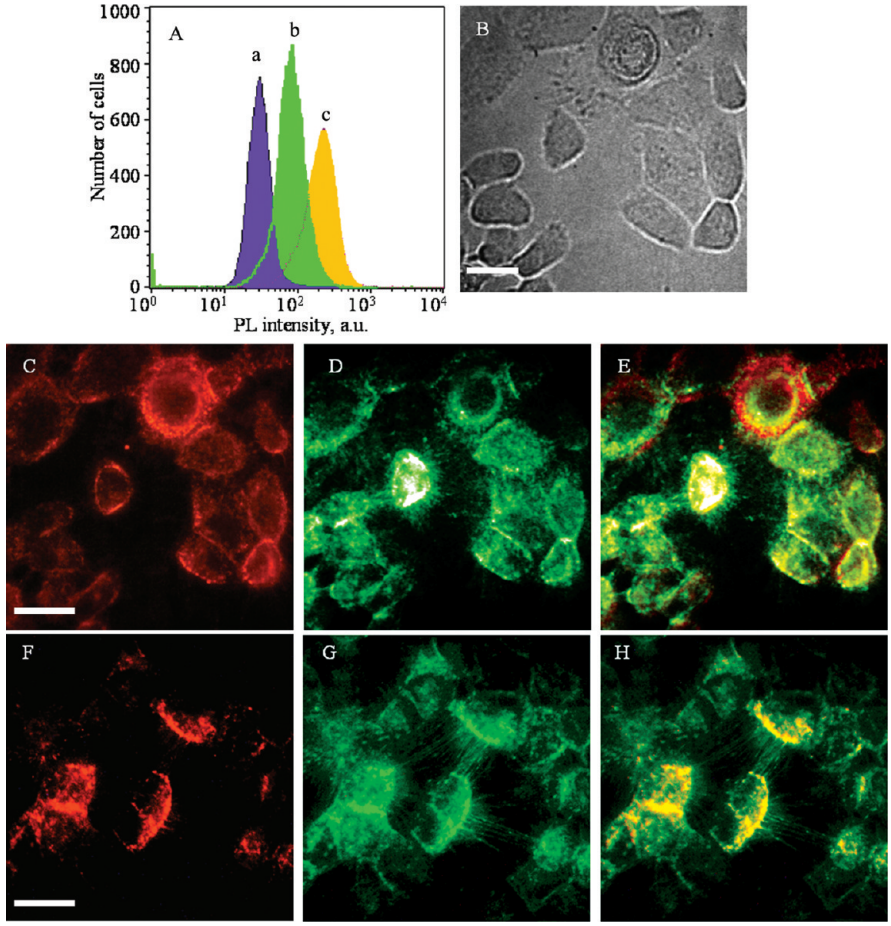

Figure 4. (A) Flow cytometry histogram of A431 cells: (a) scattering from unlabeled cells, (b) fluorescence from cells labeled with QD560−antibody conjugate, and (c) fluorescence from cells labeled with QD560−antibody conjugate followed by QD605−AST1. (B) Optical transmission image and (C−E) fluorescence images of living A431 cells treated with solutions of QD560−antibody conjugate followed by QD−AST1. (F−H) Fluorescence images of fixed A431 cells; the cells were treated with QD605−AST1 before permeabilizing the cell membrane and QD560−antibody conjugate after permeabilizing the cell membrane. (C,F) Fluorescence images acquired through a band-pass filter for QD605, (D,G) fluorescence images acquired through a band-pass filter for QD560, and (E,H) overlaid images. The scale bars are 25 μm. Note that all of the images were equally corrected for brightness and contrast.

and 3T3 cells by preincubating the cells with a galanin antagonist. Here, we investigated the role of galanin receptors in the intracellular delivery of QD−AST1 in A431 and 3T3 cells because DAR 1 and DAR 2 receptors of AST1 in insects and crustaceans show functional and sequence similarity to galanin receptors in mammalian cells.[66,68] Figure 6A,B shows the flow cytometry histograms and fluorescence images of A431 and 3T3 cells incubated with QD−AST1 after blocking galanin receptors with galanin antagonist. Also, bar c in Figure 3A,B shows the efficiency for the intracellular delivery of QD−AST1 in A431 and 3T3 cells after blocking galanin receptors. The intracellular delivery of QD−AST1 in A431 and 3T3 cells blocked with the antagonist was decreased by 8 ± 3% compared with unblocked cells, indicating that galanin receptors contributed only a little to the intracellular delivery of QD−AST1. To confirm the role of galanin receptors in the intracellular delivery of QD−AST1, we further recorded and analyzed the flow cytometry histograms of cells blocked with different concentrations of the antagonist. Typically, the cells were preincubated with 1−1000 nM antagonist solutions for 30 min, copiously washed with PBS, and incu-

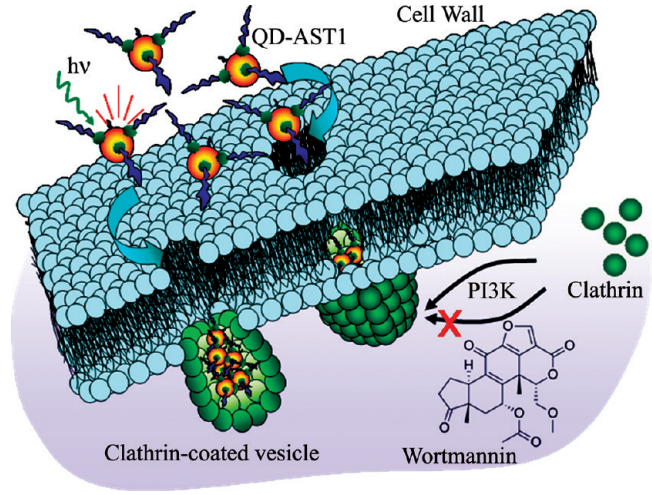

Figure 5. Schematic presentation of clathrin-mediated endocytosis of QD−AST1 conjugates, and the inhibition of PI3K enzyme by wortmannin.

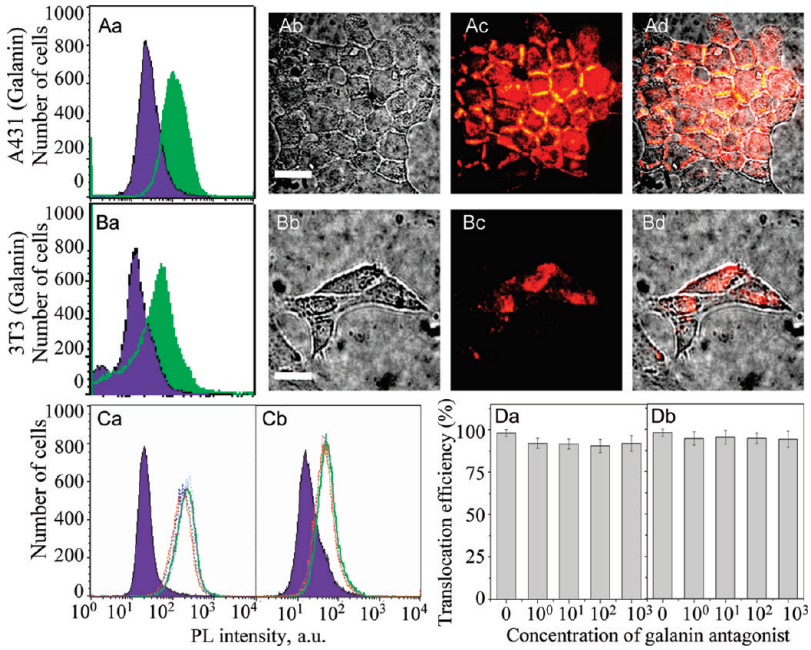

Figure 6. (Aa,Ba) Flow cytometry histograms, (Ab,Bb) optical transmission images, (Ac,Bc) fluorescence images, and (Ad,Bd) overlaid images of A431 (panel A) and 3T3 (panel B) cells incubated with 100 nM galanin antagonist solutions followed by 1 nM QD−AST1 solutions. (C) Flow cytometry histograms of (Ca) A431 and (Cb) 3T3 cells preincubated with 0, 1, 10, 100, and 1000 nM galanin antagonist solutions followed by a 1 nM QD−AST1 solution. (D) Histograms of fluorescence intensities from (Da) A431 and (Db) 3T3 cells preincubated with 0−1000 nM galanin antagonist solutions followed by a 1 nM QD−AST1 solution. The scale bars are 25 μm. Note that all of the images were equally corrected for brightness and contrast.

bated with 1 nM QD−AST1 for 30 min. Figure 6C,D shows the flow cytometry histograms of the cells incubated with 0, 1, 10, 100, and 1000 nM antagonist solutions followed by a 1 nM QD−AST1 solution. We found that the efficiency for the intracellular delivery of QD−AST1 was initially decreased by 8 ± 3% at 1 nM antagonist concentration and remained essentially unaffected up to 1000 nM (Figure 6D), suggesting that the contribution of galanin receptors to the intracellular delivery of QD−AST1 is not significant. Although galanin receptors are expressed in neurons, lung cancers, glioma, prostate cancer, *etc.*, the levels of galanin and galanin receptors are low in A431 and 3T3 cells.[70,71] Thus, regardless of the functional and sequence similarity between the receptors of galanin in mammalian cells and AST1 in insects and crustaceans, we attribute that the poor efficiency of galanin receptor-mediated endocytosis of QD−AST1 in A431 and 3T3 cells was due to the low levels of galanin receptors in these cell lines.

To investigate whether charge-based cell penetration due to the presence of a positively charged arginine unit in AST1 contributed to the intracellular delivery of QD−AST1, we employed MAST1, a mutant of AST1, in which the arginine unit was replaced with an alanine unit. We estimated the efficiency for the intracellular delivery of QD−MAST1 using flow cytometry and fluorescence microscopy and compared the efficiencies for QD−MAST1 and QD−AST1. Panels A and B in Figure 7 show the flow cytometry histograms and fluorescence images of A431 and 3T3 cells incubated with 1 nM QD−MAST1 solutions. Also, bars a and d in Figure 3 show the efficiencies for the intracellular delivery of QD−AST1 and QD−MAST1, respectively. We observed that the intracellular delivery of QD−MAST1 was lower (by 13 ± 4% in A431 and 27 ± 4% in 3T3) than that of QD−AST1. Also, the fluorescence intensity for the cells treated with QD−MAST1 (Figure 7A,B) was lower than that for cells treated with QD−AST1 (Figure 2A,C). The difference between the intracellular delivery of QD−AST1 and QD−MAST1 suggested that arginine in AST1 contributed to the intracellular delivery of QD−AST1.

To further investigate the role of positive charge due to an arginine unit in AST1 on the intracellular delivery of QD−AST1, we treated the cells with heparinase enzyme, which suppresses the negative charge on the plasma membrane by depleting glycosaminoglycan (heparan sulfate). Here, we preincubated A431 and 3T3 cells with 0.5 U heparinase enzyme solutions, copiously washed the cells with PBS, and incubated with 1 nM QD−AST1 solutions. Panels C and D in Figure 7 show the flow cytometry histograms and fluorescence images of A431 and 3T3 cells incubated with heparinase enzyme solutions followed by QD−AST1 solutions. Also, bars a and e in Figure 3 show the efficiencies for intracellular delivery of QD−AST1 before and after incubating the cells with heparinase enzyme. We found that the efficiencies were decreased by 18 ± 7 and 30 ± 4%, respectively, for A431 and 3T3 cells incubated with heparinase enzyme, suggesting that the negative charge of the plasma membrane due to heparan sulfate contributed to the intracellular delivery of QD−AST1. The efficiencies for the intracellular delivery of QD−AST1 in cells preincubated with heparan sulfate and of QD−MAST1 in untreated cells were comparable. These results suggested that an electrostatic interaction between positively charged arginine moiety in QD−AST1 and negatively charged plasma membrane was involved in the intracellular delivery of QD−AST1. Although the role of arginine in the intracellular delivery of peptides is a matter of considerable debate, the current work supports earlier reports on efficient intracellular delivery of arginine-rich peptides.[38,69,72,73] In general, arginine-rich peptides internalize through fusion with the plasma membrane. This fusion transiently destabilizes the membrane, creates pores in the membrane and translocates the peptides.[73] On the basis of the low efficiencies for the intracellular delivery of QD−MAST1 in normal cells and QD−AST1 in heparan sulfate treated cells, we attribute that charge-based cell

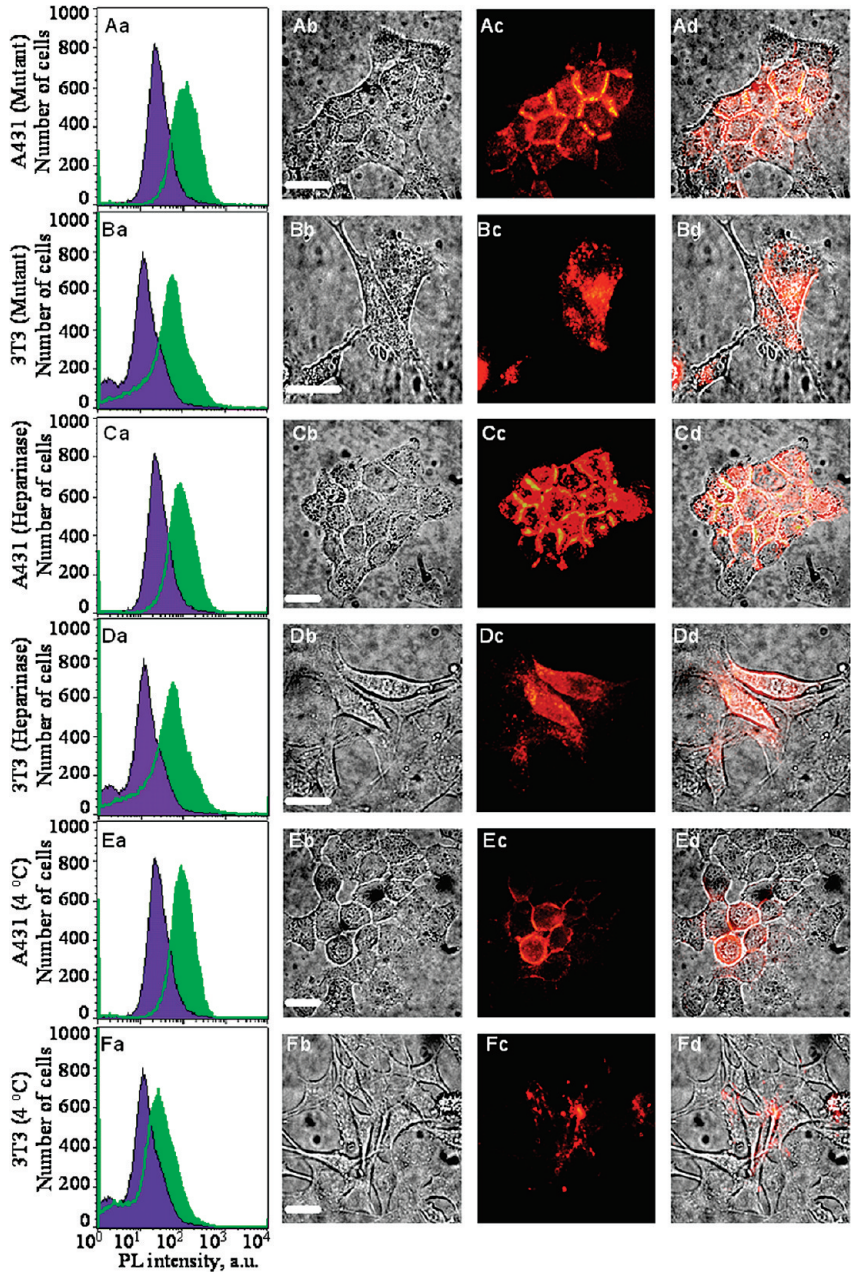

Figure 7. (Column a) Flow cytometry histograms, (column b) optical transmission images, (column c) fluorescence images, and (column d) overlay images of A431 and 3T3 cells: (panel A) A431 cells incubated with a 1 nM QD−MAST1 solution, (panel B) 3T3 cells incubated with a 1 nM QD−MAST1 solution, (panel C) A431 cells incubated with a 0.5 U heparinase enzyme followed by 1 nM QD−AST1, (panel D) 3T3 cells incubated with 0.5 U heparinase enzyme followed by a 1 nM QD−AST1 solution, (panel E) A431 cells incubated with a 1 nM QD−AST1 solution at 4 °C, and (panel F) 3T3 cells incubated with a 1 nM QD−AST1 solution at 4 °C. The scale bars are 25 μm. Note that all of the images were equally corrected for brightness and contrast.

penetration cannot be underestimated in the intracellular delivery of QD−AST1.

Transduction but endocytosis is an energy-independent process unaffected at low temperatures. Thus, to verify transduction, we examined the intracellular delivery of QD−AST1 at 4 °C. Panels E and F in Figure 7 show the flow cytometry histograms and fluorescence images of A431 and 3T3 cells incubated with QD−AST1 at 4 °C. Also, bars a and f in Figure 3 show the efficiency for the intracellular delivery of QD−AST1 at 37 and 4 °C. We estimated the efficiencies of intracellular delivery at 4 °C to be 87 ± 4% for A431 and 55 ± 3% for 3T3 cells, suggesting that transduction was involved in the intracellular delivery of QD−AST1. The difference in the efficiencies of the intracellular delivery between A431 and 3T3 cells was probably due to difference in the cell structure and physiology. Also, the higher efficiency for A431 cells was contributed by nonspecific binding of QD−AST1 to the cell membrane, apparent in the fluorescence images (Figure 7Ec,Fc). Despite the quantitative difference in the intracellular delivery between A431 and 3T3 cells, the low efficien-

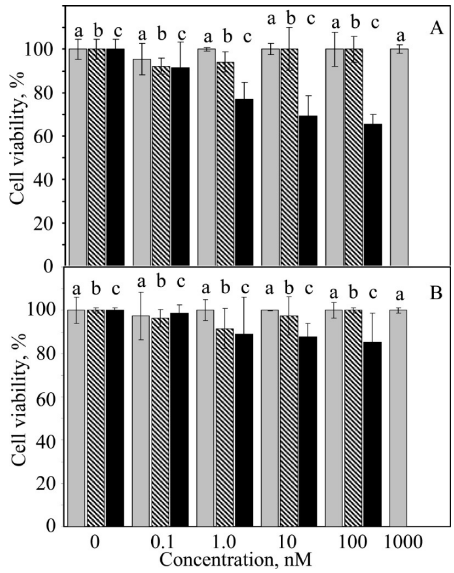

Figure 8. Histograms of MTT assays for (A) A431 and (B) 3T3 cells incubated with (a) AST1, (b) QD−streptavidin, and (c) QD−AST1.

cies for both the cells lines at 4 °C suggested that both endocytosis and transduction contributed to the intracellular delivery of QD−AST1.

It is important to analyze how toxic the internalized QD−AST1 and AST1 is before evaluating the relevance of their intracellular delivery for *in vivo* applications.[47,74] Thus, we examined the cytotoxicity of QDs, QD−AST1, and AST1. Figure 8 shows the cytotoxicity assays for A431 and 3T3 cells in the presence of AST1, QDs, and QD−AST1. Here, we separately incubated the cells with 0.1−100 nM solutions of QD, AST1 (up to 1 μM), and QD−AST1 and analyzed both the mitochondrial impairment by 3-(4,5-dimethylthiazole-2-yl)-2,5-diphenyltetrazolium (MTT) assay and the cell membrane integrity by lactate dehydrogenase (LDH) enzyme assay. On the basis of MTT assay, we found that the viability of both the cell lines was decreased, more for A431 cells (Figure 8A), with increase in the concentration of QD−AST1, but LDH assays were negative (not shown). Note that the cell viability was not affected by up to 100 nM QD (bar a, Figure 8) and 1 μM AST1 (bar b, Figure 8) concentrations. In MTT assay, we measured the cell viability in terms of the intracellular reduction of yellow MTT into purple formazan. MTT assay is standard for quantifying the redox activity of mitochondrial dehydrogenase enzyme in living cells, and any decrease in the reduction of MTT is an index of mitochondrial damage and cell death. In LDH assay, we measured LDH released from the cytoplasm into the culture fluid. LDH assay is standard for quantifying the leakage of LDH and detecting the cell wall integrity. Thus, the decrease in the cell viability in MTT assay but not in LDH assay suggested that the internalized QD−AST1 was toxic, especially at elevated levels in A431 cells (Figure 8A), probably due to an increase in the intracellular oxidative stress and not due to the lose of cell wall integrity. On the other hand, AST1 is essentially nontoxic (bar a, Figure 8). In contrast to AST1, cell-penetrating peptides derived from bacterial toxins, neural peptides, and the translocation domains of viral proteins reduce the cell viability by destabilizing the plasma membrane.[73] For example, Tat induces cytotoxicity due to membrane perturbations in HeLa cells. Cytotoxicity of QDs depends on many factors including their surface functional groups,[46,47,74] and it is a matter of great concern for advancing the applications of QDs *in vivo*. In addition to the clathrin-mediated endocytosis of QD−AST1, the current work shows that AST1 has great potential as a carrier of nanoparticles and therapeutic macromolecules *in vivo*.

In conclusion, we show that multiple pathways such as clathrin-mediated endocytosis, galanin receptor-mediated endocytosis, and transduction are involved in the intracellular delivery of QDs by AST1 peptide. Among these pathways, clathrin-mediated endocytosis is the most important, which was characterized by inhibiting PI3K, an essential kinase for assembling clathrin protein in to clathrin-coated vesicles, and colocalizing QD605−AST1 and QD560−clathrin heavy-chain antibody conjugates. Also, we characterized the roles of galanin receptor-mediated endocytosis and charge-based cell penetration in the intracellular delivery of QD−AST1 by blocking the cells with a galanin antagonist, removing the positive charge of AST1 due to arginine and suppressing the negative charge of cell membrane due to heparan sulfate. The current work suggested not only the importance of clathrin-mediated endocytosis in the intracellular delivery of peptides and peptide-conjugated nanoparticles but also the potentials of invertebrate bioresources for imaging and therapeutic applications when integrated with nanoparticles and macromolecules.

EXPERIMENTAL METHODS

Preparation of QD−Peptide Conjugates. Lyophilized AST1 (GenScript Corporation) was reconstituted into a 0.75 mM solution in sterile water, and it was biotinylated using a 15 mM aqueous solution of biotin NHS ester (Sigma-Aldrich) at 25 °C for 1 h. Biotinylated AST1 was purified by gel filtration on a sephadex G-25 column (Sigma) and diluted with water into a 250 nM solution. It was reacted with a 50 nM aqueous solution of QD−streptavidin ($\lambda_{em} \sim 605$ nm, Invitrogen) at 25 °C for 30 min, which provided a 50 nM solution of QD−AST1 conjugate. These steps were repeated for MAST1 and prepared a 50 nM solution of QD−MAST1 conjugate. The QD−peptide conjugates were prepared immediately before cell labeling.

Labeling Clathrin Heavy-Chain Antibody with QD560. A stock solution of the antibody (100 μL, Cell Signaling Technology) was divided into 10 μL aliquots. One portion of the antibody solution was diluted to 100 μL using sterile water and biotinylated using a solution (2 μM) of biotin 3-sulfoNHS ester at 25 °C for 30 min. Bioti-

nylated antibody was purified by gel filtration on a sephadex G-25 column (Sigma) and diluted into a 200 nM solution. It was reacted with a 200 nM aqueous solution of QD−streptavidin (λ_{em} ~ 560 nm, Invitrogen) at 25 °C for 30 min. Biotin−streptavidin reaction provided us with the QD−clathrin heavy-chain antibody conjugate.

Cell Labeling and Imaging. A431 and 3T3 cells were cultured up to ~50% confluence in 60 mm tissue culture plates or polylysine-coated chamber slides containing Dulbecco's modified Eagle's medium (DMEM, Sigma or GIBCO) supplemented with 10% heat-inactivated fetal bovine serum (FBS, Sigma or GIBCO). The cells were incubated with 0.5−1 nM solutions of QD−streptavidin, QD−AST1, or QD−MAST1 conjugates. Samples for studying the effect of low temperature on the intracellular delivery of QD−AST1 were prepared by incubating the cells with 1 nM QD−AST1 solutions at 4 °C for 30 min. Samples for studying the effects of inhibitors on the intracellular delivery of QD−AST1 were prepared by incubating the cells with solutions of 50 nM wortmannin (Biocompare Inc.) followed by 1 nM QD−AST1, 1−1000 nM galanin receptor antagonist (Sigma-Aldrich) followed by 1 nM QD−AST1, or 0.5 U heparinase enzyme III (Sigma-Aldrich) followed by 1 nM QD−AST1. Samples for studying clathrin-mediated endocytosis were prepared by incubating the cells with solutions of 1 nM QD−clathrin heavy-chain antibody followed by 1 nM QD−AST1. Samples for studying intranuclear delivery of QD−AST1 were prepared by incubating the cells with solutions of 5 μM Syto16 dye (Invitrogen) for 10 min followed by 1 nM QD−AST1 for 30 min. The cells were copiously (5 times) washed with 1× phosphate buffered saline (PBS) solution before and after each labeling. All of the labeling steps were carried out at 37 °C for 30 min in DMEM medium without FBS and phenol red unless otherwise stated.

Fluorescence images of the labeled cells were acquired in an inverted optical microscope (Olympus IX70) equipped with a 40× objective lens (Olympus-LUCPlanFl) or a 60× oil immersion TIRFM objective lens (Olympus-PlanApo), a 2.5× telescopic lens, band-pass filters for QDs and Syto16, an image intensifier (Hamamatsu-C8600), and a CCD camera (Hamamatsu-C5985 or Olympus). The samples were excited at 488 nm using a cw laser (Coherent Sapphire CDRH-LP).

Flow Cytometry Analysis of Cells. Cells were cultured in DMEM medium supplemented with 10% FBS for 3 days in 100 mm tissue culture plates. These cells were labeled as described above. The labeled cells were copiously washed with PBS and harvested by adding a 10× trypsin/EDTA mixture (Sigma). Trypsin was inactivated with a DMEM+FBS mixture, and the cells were suspended in BPS and collected as pellets by centrifugation (3000 rpm for 3 min). The pellets were washed three times with PBS and resuspended in DMEM without FBS and phenol red. Flow cytometry experiments were carried out on a fluorescence activated cell sorting (FACS) machine (FACSCalibur, BD Biosciences). The labeled cells were excited at 488 nm, and fluorescence signals from individual cells were collected through a band-pass filter (564−604 nm). The flow cytometry histograms were constructed for 5×10^4 to 1×10^5 cells in each experiment. We estimated the efficiencies for the intracellular delivery of QD−AST1, QD−MAST1, and QD−streptavidin by discriminating the background scattering due to unlabeled cells from the integrated fluorescence intensity due to labeled cells by using CellQuest software.

Cytotoxicity Assays. Cytotoxicity of QD, AST1, and QD−AST1 was evaluated by 3-(4,5-dimethylthiazole-2-yl)-2,5-diphenyltetrazolium chloride (MTT) and lactate dehydrogenase (LDH) assays. These assays were conducted using an MTT cell proliferation kit (Roche Diagnostics) and a CytoTox 96 kit (Promega). Here, $\sim 1 \times 10^6$ A431 and 3T3 cells were separately inoculated into 96-well tissue culture plates (FALCON) containing DMEM supplemented with 10% FBS and incubated for 48 h at 37 °C. The cells were copiously washed with PBS, and the medium was exchanged with DMEM containing different concentrations of AST1 (1 nM to 1 μM), QD (1 to 100 nM), and QD−AST1 (1 to 100 nM). The cells were incubated for 3 h at 37 °C and assayed using MTT and CytoTox 96 kits according to the instructions by the manufacturers.

Acknowledgment. V.B. is thankful to Professor Yasuo Shinohara for providing 3T3 cells and Professor D. Muraleedharan for discussions. This research was supported by a special coordination fund for Promoting Science and Technology of the Ministry of Education, Culture, Sports, Science and Technology, the Japanese Government.

Supporting Information Available: Additional details and enlarged images of Figure 4. This material is available free of charge *via* the Internet at http://pubs.acs.org.

REFERENCES AND NOTES

1. Biju, V.; Itoh, T.; Anas, A.; Sujith, A.; Ishikawa, M. Semiconductor Quantum Dots and Metal Nanoparticles: Syntheses, Optical Properties, and Biological Applications. *Anal. Bioanal. Chem.* **2008**, *391*, 2469–2495.
2. Akerman, M. E.; Chan, W. C. W.; Laakkonen, P.; Bhatia, S. N.; Ruoslahti, E. Nanocrystal Targeting *In Vivo*. *Proc. Natl. Acad. Sci. U.S.A.* **2002**, *99*, 12617–12621.
3. Frangioni, J. V. *In Vivo* Near-Infrared Fluorescence Imaging. *Curr. Opin. Chem. Biol.* **2003**, *7*, 626–634.
4. Ballou, B.; Lagerholm, B. C.; Ernst, L. A.; Bruchez, M. P.; Waggoner, A. S. Noninvasive Imaging of Quantum Dots in Mice. *Bioconjugate Chem.* **2004**, *15*, 79–86.
5. Gao, X. L.; Chen, J.; Chen, J. Y.; Wu, B. X.; Chen, H. Z.; Jiang, X. G. Quantum Dots Bearing Lectin-Functionalized Nanoparticles as a Platform for *In Vivo* Brain Imaging. *Bioconjugate Chem.* **2008**, *19*, 2189–2195.
6. Ballou, B.; Ernst, L. A.; Andreko, S.; Harper, T.; Fitzpatrick, J. A. J.; Waggoner, A. S.; Bruchez, M. P. Sentinel Lymph Node Imaging Using Quantum Dots in Mouse Tumor Models. *Bioconjugate Chem.* **2007**, *18*, 389–396.
7. Kobayashi, H.; Hama, Y.; Koyama, Y.; Barrett, T.; Regino, C. A. S.; Urano, Y.; Choyke, P. L. Simultaneous Multicolor Imaging of Five Different Lymphatic Basins Using Quantum Dots. *Nano Lett.* **2007**, *7*, 1711–1716.
8. Kim, S.; Lim, Y. T.; Soltesz, E. G.; Degrand, A. M.; Lee, J.; Nakayama, A.; Anthony Parker, J.; Mihaljevic, T.; Laurence, R. G.; Dor, D. M.; Cohn, L. H.; Bawendi, M. G.; Frangioni, J. V. Near-Infrared Fluorescent Type II Quantum Dots for Sentinel Lymph Node Mapping. *Nat. Biotechnol.* **2004**, *22*, 93–97.
9. Qian, J.; Yong, K. T.; Roy, I.; Ohulchanskyy, T. Y.; Bergey, E. J.; Lee, H. H.; Tramposch, K. M.; He, S. L.; Maitra, A.; Prasad, P. N. Imaging Pancreatic Cancer Using Surface-Functionalized Quantum Dots. *J. Phys. Chem. B* **2007**, *111*, 6969–6972.
10. Michalet, X.; Pinaud, F. F.; Bentolila, L. A.; Tsay, J. M.; Doose, S.; Li, J. J.; Sundaresan, G.; Wu, A. M.; Gambhir, S. S.; Weiss, S. Quantum Dots for Live Cells, *In Vivo* Imaging, and Diagnostics. *Science* **2005**, *307*, 538–544.
11. Al-Jamal, W. T.; Al-Jamal, K. T.; Tian, B.; Lacerda, L.; Bornans, P. H.; Frederik, P. M.; Kostarelos, K. Lipid-Quantum Dot Bilayer Vesicles Enhance Tumor Cell Uptake and Retention *In Vitro* and *In Vivo*. *ACS Nano* **2008**, *2*, 408–418.
12. Cai, W.; Shin, D.-W.; Chen, K.; Gheysens, O.; Cao, Q.; Wang, S. X.; Gambhir, S. S.; Chen, X. Peptide-Labeled Near Infrared Quantum Dots for Imaging Tumor Vasculature in Living Subjects. *Nano Lett.* **2006**, *6*, 669–676.
13. Dubertret, B.; Skourides, D.; Norris, D. J.; Noireaux, V.; Brivanlou, A. H.; Libchaber, A. *In Vivo* Imaging of Quantum Dots Encapsulated in Phospholipid Micelles. *Science* **2002**, *298*, 1759–1762.
14. Smith, B. R.; Cheng, Z.; De, A.; Koh, A. L.; Sinclair, R.; Gambhir, S. S. Real-Time Intravital Imaging of RGD−Quantum Dot Binding to Luminal Endothelium in Mouse Tumor Neovasculature. *Nano Lett.* **2008**, *8*, 2599–2606.
15. Jayagopal, A.; Russ, P. K.; Haselton, F. R. Surface Engineering of Quantum Dots for *In Vivo* Vascular Imaging. *Bioconjugate Chem.* **2007**, *18*, 1424–1433.
16. Samia, A. C. S.; Chen, X. B.; Burda, C. Semiconductor Quantum Dots for Photodynamic Therapy. *J. Am. Chem. Soc.* **2003**, *125*, 15736–15737.

17. Tsay, J. M.; Trzoss, M.; Shi, L.; Kong, X.; Selke, M.; Jung, M. E.; Weiss, S. Singlet Oxygen Production by Peptide-Coated Quantum Dot−Photosensitizer Conjugates. *J. Am. Chem. Soc.* **2007**, *129*, 6865–6871.
18. Anas, A.; Akita, H.; Harashima, H.; Itoh, T.; Ishikawa, M.; Biju, V. Photosensitized Breakage and Damage of DNA by CdSe−ZnS Quantum Dots. *J. Phys. Chem. B* **2008**, *112*, 10005–10011.
19. Bruchez, J. M.; Moronne, M.; Gin, P.; Weiss, S.; Alivisatos, P. Semiconductor Nanocrystals as Fluorescent Biological Labels. *Science* **1998**, *281*, 2013–2016.
20. Chan, W. C. W.; Nie, S. Quantum Dot Bioconjugates for Ultrasensitive Nonisotopic Detection. *Science* **1998**, *281*, 2016–2018.
21. Rajan, S. S.; Liu, H. Y.; Vu, T. Q. Ligand-Bound Quantum Dot Probes for Studying the Molecular Scale Dynamics of Receptor Endocytic Trafficking in Live Cells. *ACS Nano* **2008**, *2*, 1153–1166.
22. Nehilla, B. J.; Allen, P. G.; Desai, T. A. Surfactant-Free, Drug-Quantum-Dot Coloaded Poly(lactide-*co*-glycolide) Nanoparticles: Towards Multifunctional Nanoparticles. *ACS Nano* **2008**, *2*, 538–544.
23. Qi, L. F.; Gao, X. H. Quantum Dot-Amphipol Nanocomplex for Intracellular Delivery and Real-Time Imaging of SiRNA. *ACS Nano* **2008**, *2*, 1403–1410.
24. Joo, K. I.; Lei, Y. N.; Lee, C. L.; Lo, J.; Xie, J. S.; Hamm-Alvarez, S. F.; Wang, P. Virus Site-Specific Labeling of Enveloped Viruses with Quantum Dots for Single Virus Tracking. *ACS Nano* **2008**, *2*, 1553–1562.
25. Liu, W.; Howarth, M.; Greytak, A. B.; Zheng, Y.; Nocera, D. G.; Ting, A. Y.; Bawendi, M. G. Compact Biocompatible Quantum Dots Functionalized for Cellular Imaging. *J. Am. Chem. Soc.* **2008**, *130*, 1274–1284.
26. Medintz, I. L.; Uyeda, H. T.; Goldman, E. R.; Mattoussi, H. Quantum Dot Bioconjugates for Imaging, Labelling and Sensing. *Nat. Mater.* **2005**, *4*, 435–446.
27. Van Tilborg, G. A. F.; Mulder, W. J. M.; Chin, P. T. K.; Storm, G.; Reutelingsperger, C. P.; Nicolay, K.; Strijkers, G. J. Annexin A5-Conjugated Quantum Dots with a Paramagnetic Lipidic Coating for the Multimodal Detection of Apoptotic Cells. *Bioconjugate Chem.* **2006**, *17*, 865–868.
28. Zaman, M. B.; Baral, T. N.; Zhang, J. B.; Whitfield, D.; Yu, K. Single-Domain Antibody Functionalized CdSe/ZnS Quantum Dots for Cellular Imaging of Cancer Cells. *J. Phys. Chem. C* **2009**, *113*, 496–499.
29. Wu, X. Y.; Liu, H. J.; Liu, J. Q.; Haley, K. N.; Treadway, J. A.; Larson, J. P.; Ge, N. F.; Peale, F.; Bruchez, M. P. Immunofluorescent Labeling of Cancer Marker Her2 and Other Cellular Targets with Semiconductor Quantum Dots. *Nat. Biotechnol.* **2003**, *21*, 41–46.
30. Derfus, A. M.; Chan, W. C. W.; Bhatia, S. N. Intracellular Delivery of Quantum Dots for Live Cell Labeling and Organelle Tracking. *Adv. Mater.* **2004**, *16*, 961–964.
31. Hasegawa, U.; Nomura, S. I. M.; Kaul, S. C.; Hirano, T.; Akiyoshi, K. Nanogel−Quantum Dot Hybrid Nanoparticles for Live Cell Imaging. *Biochem. Biophys. Res. Commun.* **2005**, *331*, 917–921.
32. Yezhelyev, M. V.; Qi, L. F.; O'Regan, R. M.; Nie, S.; Gao, X. H. Proton-Sponge Coated Quantum Dots for SiRNA Delivery and Intracellular Imaging. *J. Am. Chem. Soc.* **2008**, *130*, 9006–9012.
33. Alivisatos, P.; Gu, W.; Larabell, C. Quantum Dots as Cellular Probes. *Annu. Rev. Biomed. Eng.* **2005**, *7*, 55–76.
34. Howarth, M.; Liu, W. H.; Puthenveetil, S.; Zheng, Y.; Marshall, L. F.; Schmidt, M. M.; Wittrup, K. D.; Bawendi, M. G.; Ting, A. Y. Monovalent, Reduced-Size Quantum Dots for Imaging Receptors on Living Cells. *Nat. Methods* **2008**, *5*, 397–399.
35. Derfus, A. M.; Chen, A. A.; Min, D. H.; Ruoslahti, E.; Bhatia, S. N. Targeted Quantum Dot Conjugates for SiRNA Delivery. *Bioconjugate Chem.* **2007**, *18*, 1391–1396.
36. Kim, B. Y. S.; Jiang, W.; Oreopoulos, J.; Yip, C. M.; Rutka, J. T.; Chan, W. C. W. Biodegradable Quantum Dot Nanocomposites Enable Live Cell Labeling and Imaging of Cytoplasmic Targets. *Nano Lett.* **2008**, *8*, 3887–3892.
37. Larson, D. R.; Zipfel, W. R.; Williams, R. M.; Clark, S. W.; Bruchez, M. P.; Wise, F. W.; Webb, W. W. Water-Soluble Quantum Dots for Multiphoton Fluorescence Imaging *In Vivo*. *Science* **2003**, *300*, 1434–1436.
38. Ruan, G.; Agrawal, A.; Marcus, A. I.; Nie, S. Imaging and Tracking of Tat Peptide-Conjugated Quantum Dots in Living Cells: New Insights into Nanoparticle Uptake, Intracellular Transport, and Vesicle Shedding. *J. Am. Chem. Soc.* **2007**, *129*, 14759–14766.
39. Weissleder, R.; Kelly, K.; Sun, E. Y.; Shtatland, T.; Josephson, L. Cell-Specific Targeting of Nanoparticles by Multivalent Attachment of Small Molecules. *Nat. Biotechnol.* **2005**, *23*, 1418–1423.
40. Bharali, D. J.; Lucey, D. W.; Jayakumar, H.; Pudavar, H. E.; Prasad, P. N. Folate-Receptor-Mediated Delivery of InP Quantum Dots for Bioimaging Using Confocal and Two-Photon Microscopy. *J. Am. Chem. Soc.* **2005**, *127*, 11364–11371.
41. Chen, B.; Liu, Q. L.; Zhang, Y. L.; Xu, L.; Fang, X. H. Transmembrane Delivery of the Cell-Penetrating Peptide Conjugated Semiconductor Quantum Dots. *Langmuir* **2008**, *24*, 11866–11871.
42. Duan, H. W.; Nie, S. M. Cell-Penetrating Quantum Dots Based On Multivalent and Endosome-Disrupting Surface Coatings. *J. Am. Chem. Soc.* **2007**, *129*, 3333–3338.
43. Pinaud, F.; Michalet, X.; Bentolila, L. A.; Tsay, J. M.; Doose, S.; Li, J. J.; Iyer, G.; Weiss, S. Advances in Fluorescence Imaging with Quantum Dot Bio-Probes. *Biomaterials* **2006**, *27*, 1679–1687.
44. Delehanty, J. B.; Medintz, I. L.; Pons, T.; Brunel, F. M.; Dawson, P. E.; Mattoussi, H. Self-Assembled Quantum Dot−Peptide Bioconjugates for Selective Intracellular Delivery. *Bioconjugate Chem.* **2006**, *17*, 920–927.
45. Anikeeva, N.; Lebedeva, T.; Clapp, A. R.; Goldman, E. R.; Dustin, M. L.; Mattoussi, H.; Sykulev, Y. Quantum Dot/Peptide-MHC Biosensors Reveal Strong CD8-Dependent Cooperation between Self and Viral Antigens that Augment the T Cell Response. *Proc. Natl. Acad. Sci. U.S.A.* **2006**, *103*, 16846–16851.
46. Hoshino, A.; Fujioka, K.; Oku, T.; Suga, M.; Sasaki, Y. F.; Ohta, T.; Yasuhara, M.; Suzuki, K.; Yamamoto, K. Physicochemical Properties and Cellular Toxicity of Nanocrystal Quantum Dots Depend on Their Surface Modification. *Nano Lett.* **2004**, *4*, 2163–2169.
47. Derfus, A. M.; Chan, W. C. W.; Bhatia, S. N. Probing the Cytotoxicity of Semiconductor Quantum Dots. *Nano Lett.* **2004**, *4*, 11–18.
48. Lagerholm, B. C.; Wang, M.; Ernst, L. A.; Ly, D. H.; Liu, H.; Bruchez, M. P.; Waggoner, A. S. Multicolor Coding of Cells with Cationic Peptide Coated Quantum Dots. *Nano Lett.* **2004**, *4*, 2019–2022.
49. Weng, K. C.; Noble, C. O.; Papahadjopoulos-Sternberg, B.; Chen, F. F.; Drummond, D. C.; Kirpotin, D. B.; Wang, D. H.; Hom, Y. K.; Hann, B.; Park, J. W. Q. Targeted Tumor Cell Internalization and Imaging of Multifunctional Quantum Dot-Conjugated Immunoliposomes *In Vitro* and *In Vivo*. *Nano Lett.* **2008**, *8*, 2851–2857.
50. Yong, K.-T.; Ding, H.; Roy, I.; Law, W.-C.; Bergey, E. J.; Maitra, A.; Prasad, P. N. Imaging Pancreatic Cancer Using Bioconjugated InP Quantum Dots. *ACS Nano* **2009**, *3*, 502–510.
51. Duconge, F.; Pons, T.; Pestourie, C.; Herin, L.; Theze, B.; Gombert, K.; Mahler, B.; Hinnen, F.; Kuhnast, B.; Dolle, F.; Dubertret, B.; Tavitian, B. Fluorine-18-Labeled Phospholipid Quantum Dot Micelles for In Vivo Multimodal Imaging from Whole Body to Cellular Scales. *Bioconjugate Chem.* **2008**, *19*, 1921–1926.
52. Medintz, I. L.; Pons, T.; Delehanty, J. B.; Susumu, K.; Brunel, F. M.; Dawson, P. E.; Mattoussi, H. Intracellular Delivery of Quantum Dot−Protein Cargos Mediated by Cell

Penetrating Peptides. *Bioconjugate Chem.* **2008**, *19*, 1785–1795.
53. Vu, T. Q.; Maddipati, R.; Blute, T. A.; Nehilla, B. J.; Nusblat, L.; Desai, T. A. Peptide-Conjugated Quantum Dots Activate Neuronal Receptors and Initiate Downstream Signaling of Neurite Growth. *Nano Lett.* **2005**, *5*, 603–607.
54. Zhou, M.; Nakatani, E.; Gronenberg, L. S.; Tokimoto, T.; Wirth, M. J.; Hruby, V. J.; Roberts, A.; Lynch, R. M.; Ghosh, I. Peptide-Labeled Quantum Dots for Imaging GPCRs in Whole Cells and as Single Molecules. *Bioconjugate Chem.* **2007**, *18*, 323–332.
55. Biju, V.; Muraleedharan, D.; Nakayama, K.; Shinohara, Y.; Itoh, T.; Baba, Y.; Ishikawa, M. Quantum Dot-Insect Neuropeptide Conjugates for Fluorescence Imaging, Transfection, and Nucleus Targeting of Living Cells. *Langmuir* **2007**, *23*, 10254–10261.
56. Silver, J.; Ou, W. Photoactivation of Quantum Dot Fluorescence Following Endocytosis. *Nano Lett.* **2005**, *5*, 1445–1449.
57. Rozenzhak, S. M.; Kadakia, M. P.; Tina, M.; Caserta, B. T. R. W.; Stone, M. O.; Naik, R. R. Cellular Internalization and Targeting of Semiconductor Quantum Dots. *Chem. Commun.* **2005**, *2217*, 2217–2219.
58. Morris, M. C.; Deshayes, S.; Heitz, F.; Divita, G. Cell-Penetrating Peptides: From Molecular Mechanisms to Therapeutics. *Biol. Cell* **2008**, *100*, 201–217.
59. Patel, L.; Zaro, J.; Shen, W.-C. Cell Penetrating Peptides: Intracellular Pathways and Pharmaceutical Perspectives. *Pharm. Res.* **2007**, *24*, 1977–1992.
60. Rubino, M.; Miaczynska, M.; Lippe, R.; Zerial, M. Selective Membrane Recruitment of EEA1 Suggests a Rolein Directional Transport of Clathrin-Coated Vesicles to Early Endosomes. *J. Biol. Chem.* **2000**, *275*, 3745–3748.
61. Vieira, A. V.; Lamaze, C.; Schmid, S. L. Control of EGF Receptor Signaling by Clathrin-Mediated Endocytosis. *Science* **1996**, *274*, 2086–2089.
62. Kaplan, D. R.; Whitman, M.; Schaffhausen, B.; Pallas, D. C.; White, M.; Cantley, L. C.; Roberts, T. M. Common Elements in Growth Factor Stimulation and Oncogenic Transformation: 85 kD Phosphoprotein and Phosphatidylinositol Kinase Activity. *Cell* **1987**, *50*, 1021–1029.
63. Wymann, M. P.; Bulgarelli-Leva, G.; Zvelebil, M. J.; Pirola, L.; Vanhaesebroeck, B.; Waterfield, M. D.; Panayotou, G. Wortmannin Inactivates Phosphoinositide 3-Kinase by Covalent Modification of Lys-802, a Residue Involved in the Phosphate Transfer Reaction. *Mol. Cell. Biol.* **1996**, *16*, 1722–1733.
64. Lindgren, M.; Gallet, X.; Soomets, U.; Hallbrink, M.; Brakenhielm, E.; Pooga, M.; Brasseur, R.; Langel, U. Translocation Properties of Novel Cell Penetrating Transportan and Penetratin Analogues. *Bioconjugate Chem.* **2000**, *11*, 619–626.
65. Thoren, P. E. G.; Persson, D.; Esbjorner, E. K.; Goksor, M.; Lincoln, P.; Norden, B. Membrane Binding and Translocation of Cell-Penetrating Peptides. *Biochemistry* **2004**, *43*, 3471–3489.
66. Birgul, N.; Weise, C.; Kreienkamp, H.-J.; Richter, D. Reverse Physiology in *Drosophila*: Identification of a Novel Allatostatin-like Neuropeptide and Its Cognate Receptor Structurally Related to the Mammalian Somatostatin/Galanin/Opioid Receptor Family. *EMBO J.* **1999**, *18*, 5892–5900.
67. Woodhead, A. P.; Stay, B.; Seidel, S. L.; Khan, M. A.; Tobe, S. S. Primary Structure of Four Allatostatins: Neuropeptide Inhibitors of Juvenile Hormone Synthesis. *Proc. Natl. Acad. Sci. U.S.A.* **1989**, *86*, 5997–6001.
68. Lenz, C.; Willliamson, M.; Grimmelikhuijzen, C. J. P. Molecular Cloning and Genomic Organization of a Second Probable Allatostatin Receptor from Drosophila Melanogaster. *Biochem. Biophys. Res. Commun.* **2000**, *273*, 571–577.
69. Richard, J. P.; Melikov, K.; Brooks, H.; Prevot, P.; Lebleu, B.; Chernomordik, L. V. Cellular Uptake of Unconjugated TAT Peptide Involves Clathrin-Dependent Endocytosis and Heparan Sulfate Receptors. *J. Biol. Chem.* **2005**, *280*, 15300–15306.
70. Li, R. Y.; Song, H. D.; Shi, W. J.; Hu, S. M.; Yang, Y. S.; Tang, J. F.; Chen, M. D.; Chen, J. L. Galanin Inhibits Leptin Expression and Secretion in Rat Adipose Tissue and 3T3-L1 Adipocytes. *J. Mol. Endocrinol.* **2004**, *33*, 11–19.
71. Berger, A.; Santic, R.; Kronberger, C. H.; Schilling, F. H.; Kogner, P.; Ratschek, M.; Gamper, A.; Jones, N.; Sperl, W.; Kofler, B. Galanin and Galanin Receptors in Human Cancers. *Neuropetides* **2005**, *39*, 353–359.
72. Wender, P. A.; Mitchell, D. J.; Pattabiraman, K.; Pelkey, E. T.; Steinman, L.; Rothbard, J. B. The Design, Synthesis, and Evaluation of Molecules That Enable or Enhance Cellular Uptake: Peptoid Molecular Transporters. *Proc. Natl. Acad. Sci. U.S.A.* **2000**, *97*, 13003–13008.
73. Vives, E.; Brodin, P.; Lebleu, B. A Truncated HIV-1 Tat Protein Basic Domain Rapidly Translocates through the Plasma Membrane and Accumulates in the Cell Nucleus. *J. Biol. Chem.* **1997**, *272*, 16010–16017.
74. Kirchner, C.; Liedl, T.; Kudera, S.; Pellegrino, T.; Javier, A. M.; Gaub, H. E.; Stolzle, S.; Fertig, N.; Parak, W. J. Cytotoxicity of Colloidal CdSe and CdSe/ZnS Nanoparticles. *Nano Lett.* **2005**, *5*, 331–338.